

Microsolvation of the Sr^{2+} ion and its interactions with the brucite [001] surface

A. Kerridge and N. Kaltsoyannis
 Department of Chemistry, University College London
 (correspondence: n.kaltsoyannis@ucl.ac.uk)

ABSTRACT

Density functional theoretical (DFT) methods have been employed to study i) the gas- and aqueous-phase microsolvation of the strontium dication, ii) the brucite [001] surface and iii) surface complexation of the Sr^{2+} hydrates. Sequential bond enthalpies, entropies and free energies obtained for gas-phase hydrates are in excellent agreement with experiment. Inclusion of an explicit second solvation shell and a continuum bulk solvent model reveals an increased coordination of the Sr^{2+} ion, in broad agreement with experiment. An embedded cluster approach using embedding charges obtained from natural bond order analysis results in a more accurate description of the brucite [001] surface than that obtained using formal charges. Preliminary investigations into Sr^{2+} hydrate complexation with the brucite surface reveals a strong sensitivity to initial geometries and coordination number, suggesting a statistical approach may be required to characterise the surface complexes.

INTRODUCTION

The storage of intermediate level nuclear waste (ILW) containing spent uranium nuclear fuel and magnox fuel casings at the Sellafield nuclear processing plant in the UK currently takes the form of strongly alkaline storage tanks in which the ILW is immersed. After a period of several decades the primary radionuclides present in such storage ponds are ^{238}U and two of its fission products, ^{90}Sr and ^{137}Cs . Also present is sludge composed of the mineral brucite ($\text{Mg}(\text{OH})_2$) and produced by the corrosion of the magnox fuel casings. Brucite has a hydroxide terminated reactive surface which readily adsorbs both strontium and some actinides [1,2]. The understanding of the relative energetics of the surface-complexed and aqueous hydrated species is therefore becoming of critical importance with regard to strategies for the continued storage and immobilisation of radionuclides in the ILW, particularly since some of these storage ponds are nearing the end of their operational lifetimes.

Studies of the gas-phase hydration of cations are important as a step towards the understanding of the microsolvation of such ions in aqueous environments, and there is now highly accurate high pressure mass spectrometry (HPMS) data in the literature on the sequential bond enthalpies (SBH), entropies (SBS) and free energies (SBG) associated with the reaction $\text{Sr}^{2+}(\text{H}_2\text{O})_{n-1} + \text{H}_2\text{O} \rightarrow \text{Sr}^{2+}(\text{H}_2\text{O})_n$ for $6 \leq n \leq 13$ [3]. More recently, SBHs,

SBSs and SBGs obtained from threshold collision-induced dissociation (TCID) data have been reported for smaller hydrates ($1 \leq n \leq 6$) [4].

Experiments in the aqueous phase are also of great relevance to the understanding of microsolvation, since they directly probe the solvation shells of saturated species. It is found that the coordination number (CN) of the Sr dication increases in solution from its gas-phase value of 6. There is, however, significant variation in the experimental results, with values ranging from 7.3 [5] to 10.3 [6] from extended X-ray absorption fine structure (EXAFS) data, whilst most studies report a coordination number of approximately 8.

Here we apply density functional methods to study the gas phase hydration of the Sr^{2+} ion. We use these results as the basis for a study of Sr^{2+} coordination in the aqueous phase, modelling bulk water using the conductor-like screening model (COSMO) and considering the effect of an explicit second solvation shell. We also present details of our computational model of the brucite [001] surface, and give some preliminary results regarding the surface complexation of Sr^{2+} hydrates.

COMPUTATIONAL DETAILS

All calculations were performed with version 6.0 of the TURBOMOLE code using resolution-of-the-identity density functional theory (RIDFT) with the exchange-correlation functional approximated by the TPSS functional of Perdew and coworkers, which employs the meta generalised gradient approximation (meta-GGA). For the purposes of comparison, all structures were reoptimised using the popular hybrid functional, B3LYP. The def2-TZVP basis set of polarised triple- ζ quality was used for all atoms, along with the associated Sr pseudopotential. Basis set superposition errors (BSSEs) were evaluated using the counterpoise correction, under the assumption that the studied hydrates were composed of the Sr^{2+} and $(\text{H}_2\text{O})_n$ subsystems. Gas-phase vibrational frequencies were obtained via analytical gradients in order to evaluate thermochemical properties.

Solvation effects were studied by employing the COSMO continuum solvation model. Single-point energy calculations were performed on the gas-phase optimised structures, and thermochemical properties recalculated.

RESULTS

Gas-phase hydration of the Sr^{2+} dication

Here we present our calculations of the sequential bond enthalpies $\Delta H_{(n-1,n)}$ (SBH), entropies $\Delta S_{(n-1,n)}$ (SBS) and Gibbs free energies $\Delta G_{(n-1,n)}$ (SBG) for the reactions $\text{Sr}^{2+}(\text{H}_2\text{O})_{n-1} + \text{H}_2\text{O} \rightarrow \text{Sr}^{2+}(\text{H}_2\text{O})_n$, with $2 \leq n \leq 8$. Throughout this study, we refer to hydrated complexes using the nomenclature $\text{M}^{z+}/n/m/\text{PG}$, where z represents the charge of the cation, n the number of waters in the first solvation shell, m the number of waters in the second solvation shell, and PG the point group symmetry of the complex. For brevity, the point group specification will be dropped when not relevant to the discussion.

Thermochemistry of $\text{Sr}^{2+}(\text{H}_2\text{O})_n$ with $n \leq 6$

Experimental evidence [3] suggests that the first solvation shell of Sr^{2+} is filled by six waters and that there are competing conformers for larger hydrates, where the weakly bound seventh water molecule may populate the first or, preferentially, the second solvation shell. For this reason, we briefly summarise our results of those hydrates with $n \leq 6$, before moving on to a more detailed consideration of the hepta- and octahydrates. Our B3LYP calculated results are similar to those obtained with TPSS. The mean absolute deviation from experiment (MAD) in SBH is 3.9 kJmol^{-1} with TPSS and 3.8 kJmol^{-1} with B3LYP. The MAD in SBS is $7.7 \times 10^{-3} \text{ kJmol}^{-1}\text{K}^{-1}$ with TPSS and $6.0 \times 10^{-3} \text{ kJmol}^{-1}\text{K}^{-1}$ with B3LYP. The MAD in SBG is 5.9 kJmol^{-1} with TPSS and 5.4 kJmol^{-1} with B3LYP. That the MADs are within chemical accuracy for SBH for both functionals, and close to chemical

accuracy for SBG gives us confidence when extending this methodology to the more complicated hepta- and octahydrates. For these systems, we will quote results just from our TPSS calculations.

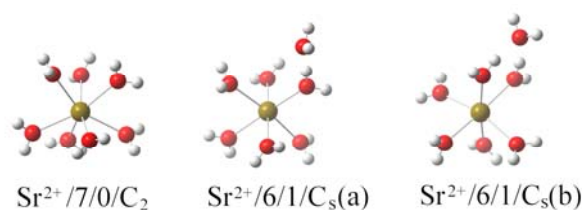


Figure 1 TPSS optimised Sr^{2+} heptahydrates

Sr^{2+} hepta- and octahydrates

We now turn our attention to Sr^{2+} microsolvated by seven and eight waters respectively, and consider a series of structures. We have identified three distinct heptahydrate structures; a heptacoordinated $\text{Sr}^{2+}/7/0/\text{C}_2$ complex and two hexacoordinated $\text{Sr}^{2+}/6/1/\text{C}_s$ complexes (Figure 1). The clear distinction between the three is the number of hydrogen bonds associated with the seventh hydrating water: 0 for $\text{Sr}^{2+}/7/0/\text{C}_2$, 1 for $\text{Sr}^{2+}/6/1/\text{C}_s(\text{a})$, and 2 for $\text{Sr}^{2+}/6/1/\text{C}_s(\text{b})$. Table 1 gives $\Delta H_{(n-1,n)}$, $\Delta G_{(n-1,n)}$ and $\Delta S_{(n-1,n)}$ for these three structures, along with the experimental values from [3].

Our results confirm the view presented in [3] that the heptahydrate should be considered as a hexacoordinated Sr^{2+} complex with the seventh water preferentially occupying the second solvation shell, but it is important to consider the sequential bond enthalpies and entropies in order to identify the experimentally observed most stable conformer. The $\text{Sr}^{2+}/6/1/\text{C}_s(\text{b})$ conformer has a large sequential bond enthalpy (over 10 kJmol^{-1} larger than the experimental value), but this is balanced by the correspondingly large sequential bond entropy, whose origin lies in the restricted rotational freedom of the doubly hydrogen-bonded second-shell water molecule. These competing contributions lead to a free energy which is comparable with that of the $\text{Sr}^{2+}/6/1/\text{C}_s(\text{a})$ conformer. Results for the $\text{Sr}^{2+}/6/1/\text{C}_s(\text{a})$ conformer are in excellent agreement with experiment, and the significantly smaller SBS in comparison with the $\text{C}_s(\text{b})$ conformer leads us to conclude that it is this conformer that is observed experimentally. The $\text{Sr}^{2+}/7/0/\text{C}_2$ conformer lies significantly higher in energy, due to the relatively small SBH and large SBS which we attribute to steric crowding in the over-filled first solvation shell.

There is a conformational entropy associated with a set of energetically similar conformers, which is not strongly sensitive to their exact energetic separation and can be well approximated by $\Delta S_{\text{mix}} \approx R \ln(n)$, where R is the gas constant and n is the number of contributing conformers [7]. We here

consider all conformers lying within ~ 10 kJmol $^{-1}$ of the most stable as contributing to ΔS_{mix} .

System	$\Delta G_{(n-1,n)}$	$\Delta H_{(n-1,n)}$	$\Delta S_{(n-1,n)}$
Sr $^{2+}$ /7/0/C $_2$	-28.8	-66.5	-0.126
Sr $^{2+}$ /6/1/C $_3$ (a)	-40.8	-72.8	-0.107
Sr $^{2+}$ /6/1/C $_3$ (b)	-39.7	-82.9	-0.145
[3], $n = 7$	-43.9 ± 2.1	-71.1 ± 4.2	-0.091 ± 0.008

Table 1 Sequential bond free energies, enthalpies and entropies of Sr $^{2+}$ heptahydrates. [11] HPMS. Energies and enthalpies in kJmol $^{-1}$, entropies in kJmol $^{-1}$ K $^{-1}$

For the heptahydrates we find $\Delta S_{\text{mix}} = 0.006$ kJmol $^{-1}$ K $^{-1}$. This reduces the sequential bond entropy from -0.107 kJmol $^{-1}$ K $^{-1}$ to -0.101 kJmol $^{-1}$ K $^{-1}$, significantly closer to the experimentally observed value of 0.091 ± 0.008 kJmol $^{-1}$ K $^{-1}$.

The conformational space spanned by potential octahydrate conformers is significantly larger than that of the heptahydrates, with much of this increase due to the Sr $^{2+}$ /6/2 conformers, where there is substantial freedom in the relative orientation of the two second shell waters. We have performed an exhaustive search of these conformers using the TPSS functional and have identified twelve stable complexes (see Figure 2), along with a series of structures exhibiting imaginary frequencies. Of the stable conformers, two are octacoordinated, two are heptacoordinated, and eight are hexacoordinated. Given the diversity of the hexacoordinated complexes, we expected to identify more than two heptacoordinated conformers, but all starting geometries led to qualitatively similar final geometries, with the second shell water H-bonding to two neighbouring first shell waters. Bearing in mind the extremely small free energy separation of 1.1 kJmol $^{-1}$ for the singly and doubly H-bonded hexacoordinated heptahydrates, the absence of stable singly H-bonded heptacoordinated octahydrates implies that the stabilisation due to the formation of the second hydrogen bond here must be larger than that in the heptahydrates. This may be due to the fact that the formation of the double hydrogen bond reduces the coulombic repulsion between the two coordinating first shell waters and the others, an effect felt more strongly in the sterically crowded heptacoordinated complex.

In Table 2 we present our TPSS calculated sequential bond free energies, enthalpies and entropies for the twelve identified octahydrates. The heptahydrate used for the evaluation of these properties is the Sr $^{2+}$ /6/1/C $_3$ (a) conformer. Figure 2 illustrates the conformers listed in Table 3.

The octahydrate results are qualitatively similar to those of the heptahydrates: the first solvation shell is filled by six waters, with the seventh and eighth preferentially occupying the second shell. The most stable heptacoordinated complex lies 8.8 kJmol $^{-1}$ above the lowest energy conformer, closer

than the 10.9 kJmol $^{-1}$ separation calculated for the heptahydrates. The heptacoordinated octahydrate

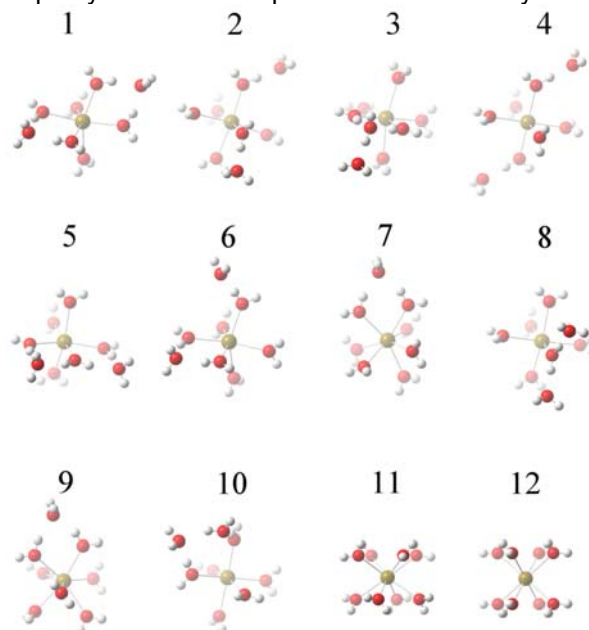


Figure 2 The twelve calculated stable Sr $^{2+}$ octahydrate complexes, ordered by TPSS-calculated sequential bond free energy.

complex contains a double H-bonded second shell water, by contrast to the heptacoordinated heptahydrate with no second shell water, and this, in conjunction with the previously mentioned associated reduction in coulombic repulsion amongst the first shell waters, leads to the relative stabilisation of the heptacoordinated octahydrate. This would also seem to be in accord with the higher CNs obtained from the aqueous phase experimental data: as the Sr $^{2+}$ ion is solvated by more waters, so the relative stability of the hexacoordinated complex is reduced. Steric crowding clearly destabilises the octacoordinated complex, which lies some 29.8 kJmol $^{-1}$ above the most stable complex.

The TPSS calculated SBG of the most stable Sr $^{2+}$ /6/2/C $_2$ (b) complex (-33.3 kJmol $^{-1}$) is in good agreement with the experimental value of -38.9 ± 2.1 kJmol $^{-1}$. However, the calculated SBH is ~ 25 kJmol $^{-1}$ larger than the experimental value, and the SBS is approximately twice that observed experimentally, leading us to conclude that this complex is being falsely stabilised by the DFT methodology used here. If we turn our attention to complex 2 of Figure 2, Sr $^{2+}$ /6/2/C $_1$ (a), we find a more likely candidate for the experimentally observed structure. Whilst the SBG (-31.7 kJmol $^{-1}$) is in poorer agreement with experiment, the SBH (-68.9 kJmol $^{-1}$) is in excellent agreement with the experimental value of -67.4 ± 4.2 kJmol $^{-1}$. There is also a large reduction in the SBS, where the calculated value, -0.125 kJmol $^{-1}$ K $^{-1}$, is in better agreement with the experimental value of -0.097 ± 0.008 kJmol $^{-1}$ K $^{-1}$. The deviation in SBG therefore appears to have its origin in the marginally overestimated SBS.

System	$\Delta G_{(n-1,n)}$	$\Delta H_{(n-1,n)}$	$\Delta S_{(n-1,n)}$
1: $\text{Sr}^{2+}/6/2/\text{C}_2(\text{b})$	-33.3	-93.5	-0.202
2: $\text{Sr}^{2+}/6/2/\text{C}_1(\text{a})$	-31.7	-68.9	-0.125
3: $\text{Sr}^{2+}/6/1/1/\text{C}_1$	-31.5	-80.2	-0.163
4: $\text{Sr}^{2+}/6/2/\text{C}_{2\text{h}}$	-31.2	-68.2	-0.126
5: $\text{Sr}^{2+}/6/2/\text{C}_{2\text{v}}$	-31.2	-89.1	-0.194
6: $\text{Sr}^{2+}/6/2/\text{C}_1(\text{c})$	-30.9	-79.5	-0.163
7: $\text{Sr}^{2+}/7/1/\text{C}_1(\text{a})$	-24.5	-74.2	-0.166
8: $\text{Sr}^{2+}/6/2/\text{C}_3(\text{a})$	-23.8	-59.3	-0.120
9: $\text{Sr}^{2+}/7/1/\text{C}_1(\text{b})$	-22.3	-73.7	-0.173
10: $\text{Sr}^{2+}/6/2/\text{C}_1(\text{b})$	-21.7	-70.4	-0.163
11: $\text{Sr}^{2+}/8/0/\text{S}_8$	-3.5	-52.1	-0.163
12: $\text{Sr}^{2+}/8/0/\text{S}_4$	19.3	-45.0	-0.216
HPMS [3]	-38.9 ± 2.1	-67.4 ± 4.2	-0.097 ± 0.008

Table 2 Sequential bond free energies, enthalpies and entropies of Sr^{2+} octahydrates. HPMS = High pressure mass spectrometry. Energies and enthalpies in kJmol^{-1} , entropies in $\text{kJmol}^{-1}\text{K}^{-1}$

With eight complexes lying within 10 kJmol^{-1} of each other, we calculate a more significant conformation entropy of $\Delta S_{\text{mix}} = 0.016 \text{ kJmol}^{-1}\text{K}^{-1}$. Inclusion of this term gives a calculated SBS of $-0.109 \text{ kJmol}^{-1}\text{K}^{-1}$, in excellent agreement with the experimental value.

COSMO solvation of octahydrates

Here we consider the four lowest energy hexacoordinated complexes (structures 1, 2, 3 and 4 of Figure 2) as calculated using TPSS, along with the lowest energy heptacoordinated (structure 7) and octacoordinated (structure 12) complexes. In Table 3 we compare the gas- and aqueous-phase relative free energies, δG . Gas-phase free energies are relative to the most stable gas phase structure, and similarly for the aqueous-phase data.

The presence of the bulk solvent leads to a substantial stabilisation of the hepta- and octacoordinated complexes, with the $\text{Sr}^{2+}/7/1/\text{C}_1(\text{a})$ complex becoming most stable. When comparing the most stable complexes with different coordination numbers, we find that the presence of the bulk solvent stabilises the heptacoordinated complex by 13.1 kJmol^{-1} relative to the hexacoordinated complex, and that the octacoordinated complex is stabilised by 14.4 kJmol^{-1} relative to the heptacoordinated and 27.5 kJmol^{-1} relative to the hexacoordinated complex. Taking a thermal average of the most stable hexa-, hepta- and octacoordinated complexes at 298K, we find a coordination number of $\text{CN} = 6.9$ in the aqueous phase, an underestimate of the value obtained experimentally, but an increase of 0.9 over the gas-phase value.

The effect of an explicit second solvation shell

Figure 3 shows the TPSS optimised $\text{Sr}^{2+}/6/12/6/\text{C}_3$, $\text{Sr}^{2+}/7/17/3/\text{C}_2$ and $\text{Sr}^{2+}/8/18/\text{S}_8$ complexes, and Table 4 compares the gas- and aqueous phases free energies of these complexes. Even in the

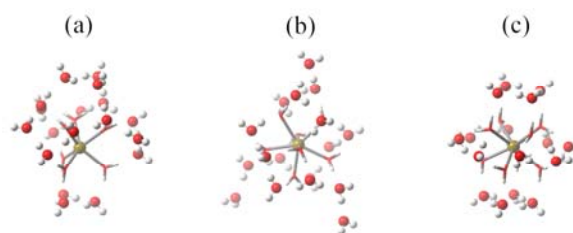


Figure 3 TPSS optimised $\text{Sr}^{2+}/6/12/6/\text{C}_3$ (a), $\text{Sr}^{2+}/7/17/3/\text{C}_2$ (b) and $\text{Sr}^{2+}/8/18/\text{S}_8$ (c) complexes. For clarity, the 1st shell waters have been rendered differently to those in subsequent shells.

Table 3 A comparison of gas- and aqueous-phase relative free energies for a selection of hexa-, hepta- and octacoordinated octahydrates. All energies are in kJmol^{-1} .

Complex	δG_{vac}	δG_{aq}
1: $\text{Sr}^{2+}/6/2/\text{C}_2(\text{b})$	0	22.4
2: $\text{Sr}^{2+}/6/2/\text{C}_1(\text{a})$	1.6	9.1
3: $\text{Sr}^{2+}/6/1/1/\text{C}_1$	1.8	4.3
4: $\text{Sr}^{2+}/6/2/\text{C}_{2\text{h}}$	2.1	14.3
5: $\text{Sr}^{2+}/7/1/\text{C}_1(\text{a})$	8.8	0
6: $\text{Sr}^{2+}/8/0/\text{S}_8$	29.8	6.6

Table 4 A comparison of gas- and aqueous-phase relative free energies for the $\text{Sr}^{2+}/6/12/6/\text{C}_3$, $\text{Sr}^{2+}/7/17/3/\text{C}_2$ and $\text{Sr}^{2+}/8/18/\text{S}_8$ complexes of Figure 3. All energies are in kJmol^{-1} .

Complex	δG_{vac}	δG_{aq}
$\text{Sr}^{2+}/6/12/6/\text{C}_3$	24.8	6.2
$\text{Sr}^{2+}/7/17/3/\text{C}_2$	0.0	0
$\text{Sr}^{2+}/8/18/0/\text{S}_8$	36.0	0.6

absence of bulk solvent, the heptacoordinated complex has become strongly stabilised relative to the hexa- and octacoordinated complexes. The effect of the solvent in this case is to significantly reduce the stability of the heptacoordinated complex; the hepta- and octacoordinated complexes are found to differ by just 0.6 kJmol^{-1} . The thermally averaged CN at 298K is 7.4, in better agreement with the experimentally obtained values.

The brucite [001] surface model

We model the brucite [001] surface using the periodic electrostatic embedded cluster method (PEECM), as implemented in TURBOMOLE. In this approach an explicit quantum mechanical cluster is embedded in an infinite array of point charges representing the bulk (see Figure 4). Typically, formal charges are used in this array, but we have found that better reconstruction of the surface is obtained by instead using charges calculated from natural bond order (NBO) analysis, which allows the polarisation of the surface hydroxyl groups to be better represented (see Figure 5). Whilst the PEECM describes long range interactions well, short-range interactions are less accurate, and so the boundary atoms of the cluster are held fixed, whilst the remaining subcluster is allowed to relax during optimisations. A stoichiometric $(\text{Mg}(\text{OH})_2)_{36}$ cluster was employed, as, unsurprisingly, only stoichiometric

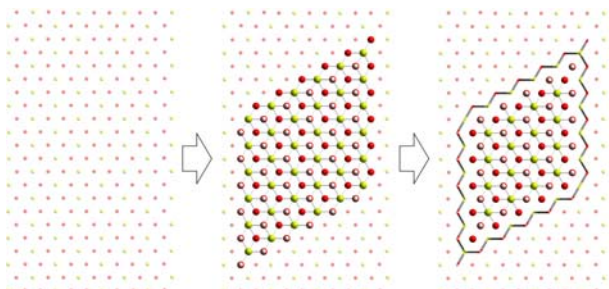


Figure 4 The PEECM brucite [001] surface model. From left to right: point charge array; embedded explicit cluster; differentiation of the fixed cluster boundary and the subcluster.

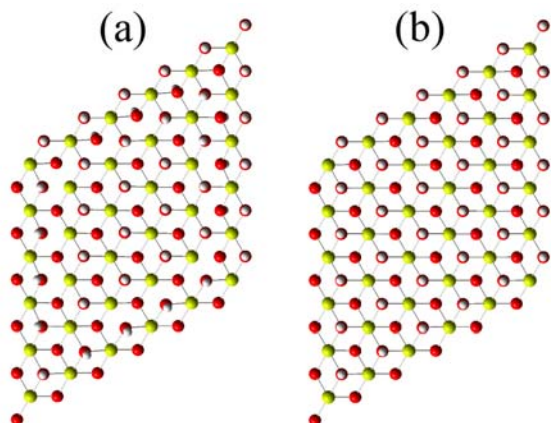


Figure 5 Brucite [001] surface optimisation. (a) formal embedding charges (Mg=+2, O=-1, H=0), (b) NBO embedding charges (Mg=+1.78, O=-1.33, H=+0.44). Note the non-orthogonality to the surface of the O-H bonds in (a).

clusters gave a simulated density of states (DOS) with a bandgap.

Surface complexation of Sr^{2+} hydrates: preliminary results

We have taken optimised hexa- hepta- and octahydrated Sr^{2+} complexes, and placed them in the vicinity of the bare brucite surface, with the Sr^{2+} ion initially located directly above a surface oxygen, and then reoptimised the complex and subcluster. Figure 6 shows the results of these optimizations. There is marked difference in the characterization of these surface complexes. In the case of the complexed hexahydrate (5a), the strontium dication is eight-coordinated, and directly coordinates three surface hydroxyl oxygens, with one water migrating into the second solvation shell. In the case of the heptahydrate (5b), the dication is five-coordinated, and there is no direct coordination with the brucite surface. Two waters migrate to the second shell, and two coordinating water are deprotonated, leading to water formation on the brucite surface. In the case of the octahydrate (5c), the dication is six-coordinated, and as with the heptahydrate, there is no direct coordination with the brucite surface and there is deprotonation of two coordinating waters.

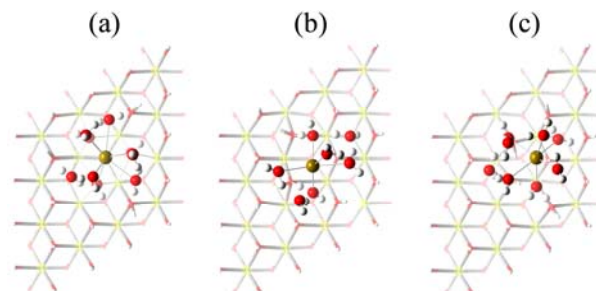


Figure 6. Examples of Sr^{2+} (a) hexa-, (b) hepta-, and (c) octahydrate complexation with the brucite [001] surface.

CONCLUSIONS AND FUTURE WORK

DFT simulations of Sr^{2+} gas phase hydration lead to highly accurate sequential bond enthalpies, entropies, and free energies. A model of solvation in the aqueous phase requires the explicit inclusion of both a second solvation shell and a continuum model for the bulk solvent in order to obtain reasonable agreement with experiment.

The PEECM has been successfully applied to model the brucite [001] surface, and the use of NBO embedding charges result in a better reconstruction of the surface than that obtained using formal charges.

Sr^{2+} hydrates appear to bind to the bare brucite [001] surface, although initial results suggest that the geometry of the hydrate relative to the surface and the coordination of the dication strongly influence the characteristics of the surface complex. Further work will be consider the effect of relative geometries in order to build a statistical description of surface complexation, and consider the interactions of solvated Sr^{2+} species with a water saturated brucite surface

REFERENCES

- 1 G. R. Bochkarev and G. I. Pushkareva, *J. Min. Sci.* **45**(3):290, 2009
- 2 J. D. Farr, P. K. Schulze, and B.D. Honeyman, *Radiochim. Acta* **88**(9-11):675, 2000
- 3 M. Peschke, A. T. Blades, and P. Kebarle, *J. Phys. Chem. A* **102**(48):9978, 1998
- 4 D. R. Carl, B. K. Chatterjee, and P.B. Armentrout, *J. Chem. Phys.* **132**(4):044303, 2010
- 5 D. M. Pfund, et al., *J. Phys. Chem.* **98**(50):13102, 1994
- 6 P. D'Angelo, H.F. Nolting, and N.V. Pavel, *Phys. Rev. A* **53**(2):798, 1996
- 7 J. P. Guthrie, *J. Phys. Chem. A*, **105**(37):8495, 2001